

Monte Carlo studies of a Finsler geometric surface model

Hiroshi Koibuchi

Department of Mechanical and Systems Engineering, Ibaraki National College of Technology, Nakane 866, Hitachinaka, Ibaraki 312-8508, Japan

Hideo Sekino

Computer Science and Engineerings, Toyohashi University of Technology, Hibarigaoka 1-1, Tenpakuchou, Toyohashi, Aichi 441-8580, Japan

Abstract

This paper presents a new type of surface models constructed on the basis of Finsler geometry. A Finsler metric is defined on the surface by using an underlying vector field, which represents an in-plane tilt order. According to the orientation of the vector field, the Finsler length becomes dependent on both position and direction on the surface, and for this reason the parameters such as the surface tension and bending rigidity become anisotropic. These parameters make the surface non-spherical. To confirm that the model is well-defined, we perform Monte Carlo simulations under several isotropic conditions such as those given by random vector fields. The results are comparable to those of previous simulations of the conventional model, which is isotropic. It is also confirmed that a tubular phase appears when the vector field is constant.

Key words: Surface model, Anisotropic membranes, Phase transition, Finsler geometry

PACS: 64.60.-i, 68.60.-p, 87.16.D-

1 Introduction

Membranes are understood as a mapping from a two-dimensional surface M to \mathbf{R}^3 [1]. If M is of sphere topology, the image $X(M)$ corresponds to a spherical membrane. The shape of $X(M)$ is governed by a surface tension energy and

Email address: koibuchi@mech.ibaraki-ct.ac.jp (Hiroshi Koibuchi).

a bending energy, which are described by a surface model of Helfrich and Polyakov (HP) [2,3]. As a general framework, the Landau-Ginzburg (LG) free energy is assumed [4,5,6]. The LG free energy includes higher order terms of the field X . Owing to such mathematical backgrounds, the surface shape and its phase structure have been extensively studied [7,8,9,10,11].

An anisotropic phase is predicted in a surface model with a bending rigidity which is anisotropic in the internal direction of the surface [12,13]. The existence of such anisotropic surface was numerically confirmed [14]. These anisotropic surface models have also been studied by non-perturbative renormalization group formalization [15]. A tubular surface can also be seen in a surface model with elastic skeleton, where a one-dimensional bending energy is assumed [16].

However, the origin of the anisotropy in membranes still remains to be clarified. Indeed, it is possible to ask why the bending rigidity becomes isotropic (or anisotropic). It is well-known that there exist anisotropic membranes without skeletons [17].

Therefore, it is interesting to study a surface model on the basis of Finsler geometry [18]. In Finsler geometry, an infinitesimal length unit is considered to be dependent on the directions, and it gives a more general framework than the Riemannian geometry. Because of this potential ability in Finsler geometry, several studies have been conducted on its applications to physics [19,20].

In this paper, a Finsler geometric (FG) surface model for membranes is studied and Monte Carlo (MC) simulation data are presented. This model is constructed by extending a discrete surface model of Helfrich and Polyakov such that the metric function is replaced by a Finsler metric. The assumed Finsler metric is defined by using a vector field \mathbf{v} on M . Since the Euclidean length of \mathbf{v} depends on the direction, this vector field \mathbf{v} is considered to be an origin of surface anisotropy. We should note that the isotropy is restored if \mathbf{v} is given locally at random. In this case, the FG model should have the same phase structure as the conventional surface model of Helfrich and Polyakov. We firstly check this under several conditions and confirm that the FG surface model is well-defined. Next, it is demonstrated that a tubular surface is obtained by assuming that \mathbf{v} is constant.

2 Finsler geometric surface model

2.1 Elements of Finsler geometry

In this subsection, we briefly summarize the elements of Finsler geometry [18]. Let M be a two-dimensional manifold, and let C be a curve on M such that $C \ni t \mapsto x(t) \in M$. We call M as a *Finsler space* if there exists a Finsler function L on M such that the Finsler length s of the curve C is given by

$$s = \int_{t_0}^t L(x, y) dt, \quad (1)$$

where $L(x, y)$ is a homogeneous function of degree 1 with respect to y . The symbols $x = (x_1, x_2)$ and $y = (y_1, y_2) = (dx_1/dt, dx_2/dt)$ in L are a point on C and a tangential vector at x with the direction along which t increases, respectively. Thus, we have

$$L(x, ky) = kL(x, y) \quad (2)$$

for any positive k . This equation implies that the Finsler length s of the curve C is independent of the parameter t . For this reason, the Finsler length s depends only on the ratio y_2/y_1 , because $y = (y_1, y_2) = y_1(1, y_2/y_1)$ can be replaced by $(1, y_2/y_1)$ in Eq. (2). We should note that the definition of Eq. (1) can also be written as

$$\frac{ds}{dt} = L(x, y). \quad (3)$$

An example of the Finsler function $L(x(t), y(t))$ is given by using a vector field \mathbf{v} such that

$$L(x(t), y(t)) = \sqrt{\sum_i y_i^2} / |\mathbf{v}|, \quad (4)$$

where $|\mathbf{v}| = \sqrt{\sum_i (dx_i/ds)^2}$. We call $\sqrt{\sum_i y_i^2}$ and $|\mathbf{v}|$ as the Euclidean lengths. Note that the reparametrization $dx_i/dt = (dx_i/ds)(ds/dt)$ allows us to write $\sqrt{\sum_i y_i^2} = \sqrt{\sum_i (dx_i/ds)^2} ds/dt$. Thus, we have $ds/dt = \sqrt{\sum_i y_i^2} / |\mathbf{v}|$. This leads to the expression s in Eq. (1). The vector \mathbf{v} along C in Eq. (4) can also be given by the y -direction component of a given vector field. In this example, the direction of \mathbf{v} needs to not always be identical to that of y and may be reverse to that of y .

Let $T_x M$ be the tangential plane at x . Then, we have a loop made of all end points of the vectors $Y \in T_x M$ satisfying

$$L(x, Y) = 1. \quad (5)$$

This equation is obtained by assuming $t=s$ in Eq. (3). Thus, we have a Finsler length scale at x such that $L(x, Y) = 1$. In the case of Eq. (4), the condition $L(x, Y) = 1$ implies that $\sqrt{\sum_i Y_i^2} = |\mathbf{v}|$. Since the length $|\mathbf{v}|$ depends on its direction, we understand that the Euclidean length $\sqrt{\sum_i Y_i^2}$ depends on its direction on the loop $L(x, Y) = 1$. To the contrary, the Finsler length of Y is constant, which is 1 in the unit of $|\mathbf{v}|$, and hence it is independent of the direction on the loop.

In the example in Eq. (4), the Euclidean length of s is given by $s|\mathbf{v}|$, which is identical with the Finsler length if $|\mathbf{v}|=1$, and hence Finsler length s along C is implicitly dependent on \mathbf{v} along the direction of y . Thus, we find that the Finsler length s defined at x on M depends both on the direction of \mathbf{v} and on the length of \mathbf{v} . Since the length of \mathbf{v} is dependent on x , the Finsler length depends on the position and the direction.

2.2 Finsler length on triangulated surfaces

We assume that M is smoothly or piece-wise linearly triangulated such that the Euclidean bond lengths are given. On the triangulated surfaces, the vertices, the bonds, and the triangles are independently labeled by sequential numbers. Let N, N_B, N_T be the total number of vertices, the total number of bonds, and the total number of triangles. One additional assumption is that the bond ij , which is connecting two neighboring vertices i and j , is labeled also by velocities or velocity magnitudes v_{ij} and v_{ji} , which are positive. We should note that $v_{ij} \neq v_{ji}$ in general and that v_{ij} plays a role of the unit of Finsler length from i to j . Thus the bonds are labeled not only by a series of integers $1, 2, \dots, N_B$ but also by two series of positive real numbers v_1, v_2, \dots, v_{N_B} and $v'_1, v'_2, \dots, v'_{N_B}$. It is also possible to assume that $v_i = v'_i$.

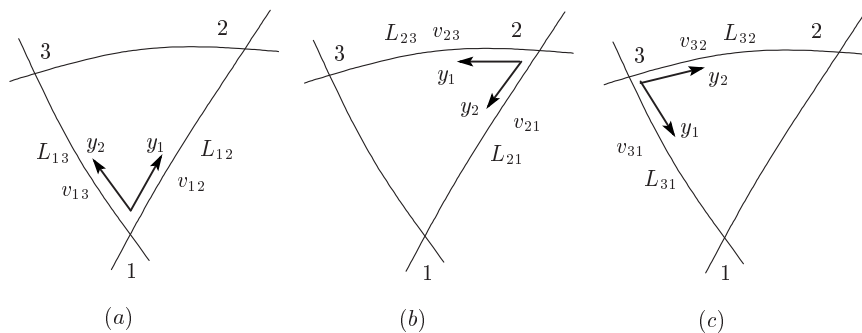


Fig. 1. A smooth triangle Δ in M with a local coordinate (a) at the vertex 1, (b) at vertex 2, and (c) at the vertex 3.

We should comment on a natural assumption that each triangle is labeled by a single local coordinate. Indeed, we have three possible local coordinates on a triangle, and the total number of coordinates is $3N_T$ for a given triangulation

of M . Thus, we chose a set of N_T coordinates from those possible 3^{N_T} ones. The three possible coordinate systems of a triangle Δ are shown in Figs. 1(a)–1(c). In Fig. 1(a), the local coordinate of Δ is denoted by (x_1, x_2) such that the origin of the coordinate axes coincides with the vertex 1. The velocity parameters v_{12} and v_{13} are defined along y_1 and y_2 respectively so that the direction of v_{12} (v_{13}) from 1 to 2 (1 to 3) coincides with the direction of y_1 (y_2). Note that the velocity v_{21} is not included in the coordinate system in Fig. 1(a), while it is included in Fig. 1(b).

Note that the two different velocity v_i and v'_i can be obtained from a smooth and non-constant vector field \mathbf{v} on the surface. Indeed, suppose that \mathbf{v} has value only on the vertices of the triangulated surface. In such case (see Fig. 1(a)), if the local coordinate origin is located at the vertex 1, the value v_{12} can be obtained from $\mathbf{v}(1)$ at the vertex 1. On the contrary, v_{21} is obtained from $\mathbf{v}(2)$ in the case of Fig. 1(b). If \mathbf{v} is not constant, then $\mathbf{v}(1) \neq \mathbf{v}(2)$, and therefore we have $v_{12} \neq v_{21}$ in general.

We firstly define a Finsler function $L(x, y)$ on Δ in Fig. 1(a) such that

$$L(x, y) = \begin{cases} y_1/v_{12} & \text{(on the } x_1 \text{ axis),} \\ y_2/v_{13} & \text{(on the } x_2 \text{ axis).} \end{cases} \quad (6)$$

Thus the Finsler length L_{12} of the bond 12 is given by $L_{12} = L_1/v_{12}$. Indeed, $L_{12} = \int_1^2 L(x, y) dt = \int_1^2 (1/v_{12}) y_1 dt = (1/v_{12}) y_1 \Delta t = (1/v_{12}) dx_1$. This proves $L_{12} = L_1/v_{12}$ because $dx_1 = L_1$, where L_1 is the Euclidean length of the bond 12. It is also easy to see that $L_{13} = L_2/v_{13}$.

Secondly, we define a Regge metric [21,22,23] on Δ in Fig. 1(a) such that

$$g_{ab}^R = \begin{pmatrix} L_1^2 & F_3 \\ F_3 & L_2^2 \end{pmatrix}, \quad F_3 = L_1 L_2 \cos \Phi_3, \quad (7)$$

where Φ_3 is the internal angle of the vertex 1. The triangular relation such as $L_i + L_j > L_k$ is assumed. We should note that $\sum_{i=1}^3 \Phi_i$ is not always constrained to be π . For this reason, a deficit angle φ is defined on the triangle Δ such that $\varphi = \sum_{i=1}^3 \Phi_i - \pi$ [24]. Equivalently, the internal angle Φ_i is obtained from φ such that $\Phi_i = \Phi_i^0 (1 + \varphi/\pi)$, ($i = 1, 2, 3$), where $\sum_{i=1}^3 \Phi_i^0 = \pi$. We assume in this paper that the variables Φ_i ($i = 1, 2, 3$), and hence the variables F_i ($i = 1, 2, 3$), are independent to each other for the numerical simplicity. Note that g_{ab}^R reduces to the Euclidean metric δ_{ab} if $L_1 = L_2 = 1$ and $F_3 = 0$.

Note also that the Euclidean edge length L_i is independent of the local coordinate, while the Regge metric g_{ab}^R itself depends on the coordinate. For this reason, the discrete Hamiltonian is obtained by using three different g_{ab}^R cor-

responding to three different coordinates at each triangle in the conventional model.

By replacing L_1 by L_{12} and L_2 by L_{13} in the Regge metric g_{ab}^R in Eq. (7), we have a Finsler metric g_{ab}^F such that

$$g_{ab}^F = \begin{pmatrix} L_1^2/v_{12}^2 & F_3/v_{12}v_{13} \\ F_3/v_{12}v_{13} & L_2^2/v_{13}^2 \end{pmatrix}, \quad F_3 = L_1 L_2 \cos \Phi_3. \quad (8)$$

This g_{ab}^F gives two different lengths for an edge of the triangle. Indeed, the edge length $L_{12}(=L_1/v_{12})$ with respect to the local coordinate in Fig. 1(a) is different from the one $L_{21}(=L_1/v_{21})$ with respect to the local coordinate in Fig. 1(b) because $v_{12} \neq v_{21}$. This is in sharp contrast to the case of the conventional Regge metric, where the bond length of Δ is uniquely given independent of the coordinates.

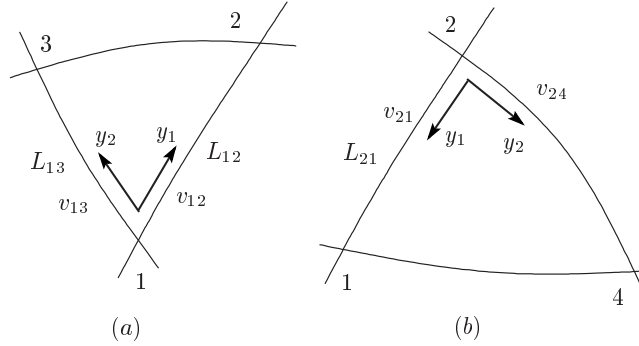


Fig. 2. (a) A triangle in M with the local coordinate origin is at the vertex 1, and (b) a neighboring triangle with the local coordinate origin is at the vertex 2. Two triangles share the bond 12.

Figures 2(a) and 2(b) show two neighboring triangles which have a common bond 12, where the vertices 1 and 2 are the origins of the two coordinates. In this case, both v_{12} and v_{21} are used to define the model. The Finsler length of the bond 12 is given by L_{12} in the triangle of Fig. 2(a), while it is given by L_{21} in the other triangle of Fig. 2(b). This is a result of the assumption that a triangle should be labeled by a single local coordinate.

The Finsler area A_Δ of Δ is given by the determinant of g_{ab}^F such that

$$A_\Delta = \frac{1}{2} \sqrt{L_1^2 L_2^2 - F_3^2 / v_{12} v_{13}} = \frac{1}{2} L_1 L_2 \sin \Phi_3 / v_{12} v_{13}. \quad (9)$$

We should note that A_Δ depends on the local coordinate. However, this does not mean that A_Δ in Eq. (9) is ill-defined. In fact, the Finsler length depends on the coordinate, it is quite natural that A_Δ depends on the coordinate.

We should note that g_{ab}^F can also be obtained from the bi-linear form

$$L_M^2 = \sum_{\Delta} L_{\Delta}^2, \quad L_{\Delta} = \sqrt{(L_1^2/v_{12}^2)y_1^2 + (L_1^2/v_{12}^2)y_2^2 + 2(F_3/v_{12}v_{13})y_1y_2} \quad (10)$$

such that

$$g_{ab}^F = \frac{1}{2} \frac{\partial^2 L_M^2}{\partial y_a \partial y_b}. \quad (11)$$

This expression implies that g_{ab}^F is a $(0, 2)$ -tensor just like an ordinary metric $g_{ab}(x)$, because y is a $(1, 0)$ -tensor and L_M^2 is a function.

From the L_M in Eq. (10), we also have the Finsler lengths L_{12} and L_{13} of the bonds 12 and 13 of Δ in Fig. 1(a). Indeed, we have $y_2 = 0$ ($y_1 = 0$) on the x_1 (x_2) axis. Thus, we find from the bi-linear form L_{Δ}^2 that the bond length of x_1 (x_2) axis is given by $L_{12} = L_1/v_{12}$ ($L_{13} = L_2/v_{13}$). We can also start with the form L_M in Eq. (10), because L_{Δ}^2 can be written as $L_{\Delta}^2 = \sum_{ab} g_{ab}^F y_a y_b$ by using g_{ab}^F in Eq. (8).

2.3 A surface model with a Finsler metric

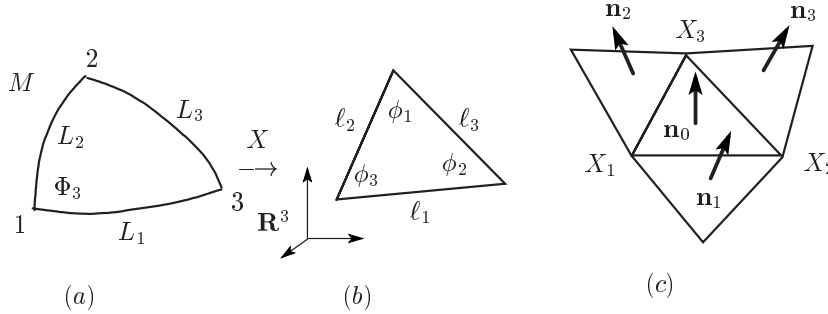


Fig. 3. (a) A smooth triangle Δ in M , (b) the image $X(\Delta)$ of Δ by a mapping X from M to \mathbf{R}^3 , and (c) a unit normal vector \mathbf{n}_0 of $X(\Delta)$ and those \mathbf{n}_i ($i=1, 2, 3$) of the nearest neighbor triangles in \mathbf{R}^3 .

In this subsection, we define a discrete model by introducing the discrete Hamiltonian and the partition function. We assume that the surface is embedded in \mathbf{R}^3 by a mapping $X : M \rightarrow \mathbf{R}^3$. A local coordinate is also assumed to be fixed on every triangle Δ in M .

A discrete Hamiltonian $S(X, g)$ is defined by

$$S(X, g) = S_1 + bS_2, \quad (12)$$

$$S_1 = \frac{1}{4} \sum_{\Delta} S_1(\Delta) / A_{\Delta}, \quad S_2 = \frac{1}{4} \sum_{\Delta} S_2(\Delta) / A_{\Delta},$$

with

$$S_1(\Delta) = \left(L_1^2/v_{12}^2\right)\ell_2^2 + \left(L_2^2/v_{13}^2\right)\ell_1^2 - 2(F_3/v_{12}v_{13})\vec{\ell}_1 \cdot \vec{\ell}_2 \quad (13)$$

and

$$S_2(\Delta) = \left(L_1^2/v_{12}^2\right)(1 - \mathbf{n}_0 \cdot \mathbf{n}_1) + \left(L_2^2/v_{13}^2\right)(1 - \mathbf{n}_0 \cdot \mathbf{n}_2) - 2(F_3/v_{12}v_{13})(\mathbf{n}_0 - \mathbf{n}_1) \cdot (\mathbf{n}_0 - \mathbf{n}_2). \quad (14)$$

The length L_i and $F_3 = L_1 L_2 \cos \Phi_3$ are the variables of Δ in M (Fig. 3(a)), while the length ℓ_i and the unit normal vectors $\mathbf{n}_i (i=1, 2)$ are those of $X(\Delta)$ in \mathbf{R}^3 (Figs. 3(b),(c)). The coefficients L_i^2/v_{jk}^2 together with $1/A_\Delta$ alter the surface tension coefficient $a(=1)$ and the bending rigidity b to be dependent on the position and direction on the surface. If v_{ij} is random and hence isotropic, the effective surface tension and bending rigidity are expected to be almost uniform and not anisotropic. To the contrary, an anisotropic v_{ij} is expected to make the coefficients anisotropic.

The discrete partition function is defined by

$$Z(b) = \int Dg \int' \prod_{i=1}^N dX_i \exp[-S(X, g)], \quad (15)$$

where

$$\begin{aligned} \int Dg = \sum_{\mathcal{C}} \int \prod_{i=1}^{N_B} dL_i \exp\left(-\lambda_L \sum_{i=1}^{N_B} L_i^2\right) \\ \int \prod_{i=1}^{N_T} dF_i \int \prod_{i=1}^{N_B} dv_i \exp\left(-\lambda_v \sum_i 1/v_i^2\right). \end{aligned} \quad (16)$$

$\int' \prod_{i=1}^N dX_i$ in $Z(b)$ denotes that the integrations are performed under the constraint that the center of mass of the surface $X(M)$ is fixed at the origin of \mathbf{R}^3 . As mentioned in the previous subsection, we use the variable F in place of φ . The integration measure $\int \prod_{i=1}^{N_T} d\varphi_i \exp\left(-\lambda_\varphi \sum_{i=1}^{N_T} |\varphi_i|\right)$, which is assumed in the model of [24], is replaced by $\int \prod_{i=1}^{N_T} dF_i$ with a constraint $|F_3| < L_1 L_2$. Under this constraint the variable F plays a role of the deficit angle $\sum_{i=1}^3 \Phi_i - \pi$ of the triangle.

The role of the factor $\exp\left(-\lambda_L \sum_{i=1}^{N_B} L_i^2\right)$ in Eq. (16), where L_i is the Euclidean bond length, is to suppress the divergence of L . The factor $\exp\left(-\lambda_v \sum_i 1/v_i^2\right)$ also prevents the variable v from being zero. The distribution of $\{v_i\}$ becomes at random and hence defines a random vector field on a surface. If the vector field \mathbf{v} is given by some other reasons externally or dynamically, this factor may be changed.

The symbol $\sum_{\mathcal{C}}$ in Eq. (16) denotes the sum over all possible coordinates \mathcal{C} . A local coordinate \mathcal{C} is fixed on Δ . In the conventional models such as the model in [24], the Hamiltonians S_1 and S_2 are defined by including the terms cyclic under permutations of three different coordinates of Δ such that $1 \rightarrow 2, 2 \rightarrow 3$, and $3 \rightarrow 1$. A permutation of three different values of \mathcal{C} is not a coordinate transformation in Δ . In fact, as \mathcal{C} changes from one to another, the discrete Hamiltonians S_1 and S_2 change. This is true not only in the conventional model but also in the Finsler geometric model. In this sense, \mathcal{C} can be viewed as a variable just like the triangulation \mathcal{T} . However, the dynamical triangulation $\sum_{\mathcal{T}}$ changes the lattice structure. Therefore, $\sum_{\mathcal{T}}$ cannot be included in $\sum_{\mathcal{C}}$.

We should emphasize that the integrations of the variables F_i and v_i depend on the coordinate \mathcal{C} . In each local coordinate of a triangle, only one of the two variables, such as v_{12} and v_{21} , is integrated. Analogously in the integrations $\int' \prod_{i=1}^{N_T} dF_i$, the variable F_i , which represents one of three different F , is integrated.

2.4 Continuous surface model

The surface model of Helfrich and Polyakov is defined by a mapping X from M to \mathbf{R}^3 such that $X : M \ni (x_1, x_2) \mapsto X(x_1, x_2) \in \mathbf{R}^3$ [1]. The symbol (x_1, x_2) denotes a local coordinate of M .

The Hamiltonian of the model is given by a linear combination of the Gaussian potential S_1 and the extrinsic curvature energy S_2 such that

$$S = S_1 + bS_2, \\ S_1 = \int \sqrt{g} d^2x g^{ab} \partial_a X^\mu \partial_b X^\mu, \quad S_2 = \frac{1}{2} \int \sqrt{g} d^2x g^{ab} \partial_a n^\mu \partial_b n^\mu, \quad (17)$$

where $b[kT]$ is the bending rigidity. The matrix $g_{ab}(a, b=1, 2)$ in S_1 and S_2 is a Riemannian metric on M , g is the determinant of g_{ab} , and g^{ab} is its inverse. The symbol n^μ in S_2 is a unit normal vector of the surface. We should note that S_2 is obtained from Polyakov's action for extrinsic curvature by assuming $g_{ab} = \partial_a X^\mu \partial_b X^\mu$ [3]. We here assume that g_{ab} is arbitrary in Eq. (17).

The surface model described by S in Eq. (17) is statistical mechanically defined by the partition function

$$Z(b) = \int Dg \int DX \exp[-S(X, g)], \quad (18)$$

where $S(X, g)$ denotes that S depends on the variables X and g . The integration symbols $\int Dg$ and $\int DX$ denote the sum over metrics g and the

mappings X . The model is characterized by the conformal invariance and the reparametrization invariance. The first is that the action S remains unchanged under a transformation $g_{ab} \rightarrow g'_{ab} = f g_{ab}$ for an arbitrary positive function $f(x)$. The second is that S remains unchanged under any local coordinate transformation $x \rightarrow x'$. The transformation $x \rightarrow x'$ changes both g and X , while the conformal transformation only changes g .

We simply deform this continuous model by replacing $g_{ab}(x)$ with a Finsler metric $g_{ab}(x, y)$, which is a four-variables function. In this new model the conformal invariance is apparently preserved even when the factor $f(x)$ is replaced by $f(x, y)$. In contrast, the reparametrization invariance is not always preserved, or in other words the reparametrization for x is not always extended to the one for $x, y(=\dot{x})$. The reason is that the parameter y is not a coordinate and is only allowed to transform according to a linear transformation corresponding to a coordinate transformation of x . However, the Finsler metric $g_{ab}(x, y)$ is formally a $(0, 2)$ -tensor just like $g_{ab}(x)$ as mentioned just below Eq.(11). Therefore, the continuous actions with a Finsler metric remains a scalar and hence are well-defined as action functionals.

The discrete Hamiltonians in Eqs. (12)–(14) are obtained from the continuous actions S_1 and S_2 in Eq. (17) on the triangulated surface by the replacements $\partial_1 X^\mu \rightarrow X_2^\mu - X_1^\mu$, $\partial_2 X^\mu \rightarrow X_3^\mu - X_1^\mu$, where X_i^μ denotes the position of the vertex i such that $\ell_1 = |X_2^\mu - X_1^\mu|$, $\ell_2 = |X_3^\mu - X_1^\mu|$ (see Figs. 3(a)–3(c)). The derivatives in S_2 in Eq. (17) can also be discretized by $\partial_1 n^\mu \rightarrow \mathbf{n}_0 - \mathbf{n}_2$, $\partial_2 n^\mu \rightarrow \mathbf{n}_0 - \mathbf{n}_1$, where $\mathbf{n}_i (i=1, 2, 3)$ are the unit normal vectors shown in Fig. 3(c).

3 Simulation results

3.1 Euclidean model

The model introduced in Subsection 2.3 is meaningful even in the case where the velocity parameter is fixed such that $v_{ij} = 1$ for all ij and $g_{ab}^R = \delta_{ab}$ or $g_{ab}^R = \partial_a X^\mu \partial_b X^\mu$. Indeed, the models in those cases are still not always identical to the corresponding conventional models because of \sum_C in Eq. (16). Therefore, in order to see the influence of \sum_C on the phase structure, we study not only a non-trivial Finsler geometric model but also the most simple model with $v_{ij} = 1$ and $g_{ab}^R = \delta_{ab}$.

The so-called crumpling transition between the smooth spherical phase at high bending region and the collapsed phase at low bending region has long been studied theoretically and numerically [7,8,9,10,25,26,27]. Both of the phases separated by this transition are isotropic in the sense that the surfaces are

symmetric under arbitrary three-dimensional rotations.

To see whether this transition is not influenced by the Finsler geometric treatment, we firstly study the most simple model, which is defined by

$$Z(b) = \sum_{\mathcal{C}} \int' \prod_{i=1}^N dX_i \exp[-(S_1 + bS_2)],$$

$$S_1 = \sum_{ij} (X_i - X_j)^2, \quad S_2 = \sum_{ij} (1 - \mathbf{n}_i \cdot \mathbf{n}_j). \quad (19)$$

As mentioned above, this model is identical with the conventional model except $\sum_{\mathcal{C}}$ in $Z(b)$. The Hamiltonians are discretized on a spherical lattice, which is characterized by $(N, N_B, N_T) = (10\ell^2 + 2, 30\ell^2, 20\ell^2)$, where ℓ is the number of partitions of an edge of the icosahedron.

The canonical Metropolis Monte Carlo technique is used to update the variables. The update $X' = X + \delta X$ is accepted with probability $\text{Min}[1, \exp(-\delta S')]$, $\delta S' = S'(\text{new}) - S'(\text{old})$, where δX is a random three-dimensional vector in a small sphere. The radius of this sphere is fixed to a constant to make the acceptance rate of X approximately 50%.

The sum over coordinates $\sum_{\mathcal{C}}$ in $Z(b)$ is performed as follows: On a triangle Δ , the coordinate is characterized by its origin, and hence Δ has only three possible coordinates. Therefore, the current coordinate of Δ is randomly updated to one of the two remaining coordinates. In this update of \mathcal{C} , S_1 and S_2 change from the expressions in Eqs. (13) and (14) to those cyclic under the permutations $1 \rightarrow 2, 2 \rightarrow 3$, and $3 \rightarrow 1$, and so on.

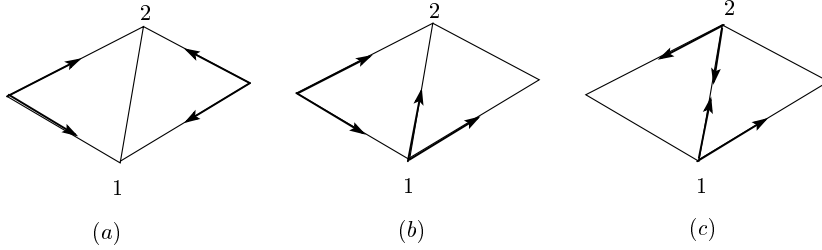


Fig. 4. Three configurations of coordinate axes in two neighboring triangles. Neither the bending energy nor the bond potential is given to the bond 12 in the coordinate of (a), while both of the energies are redundantly given to the bond 12 in the coordinate of (c).

No constraint is imposed on the update of \mathcal{C} . As a consequence, the configuration like the one in Fig. 4(a) appears, where the bond 12 shares neither S_1 nor S_2 . Thus, the random update of \mathcal{C} makes the configuration non-uniform in the sense that the distributions of S_1 and S_2 are non-uniform. Therefore, it is non-trivial whether the phase structure of the conventional model is influenced by $\sum_{\mathcal{C}}$ in Z .

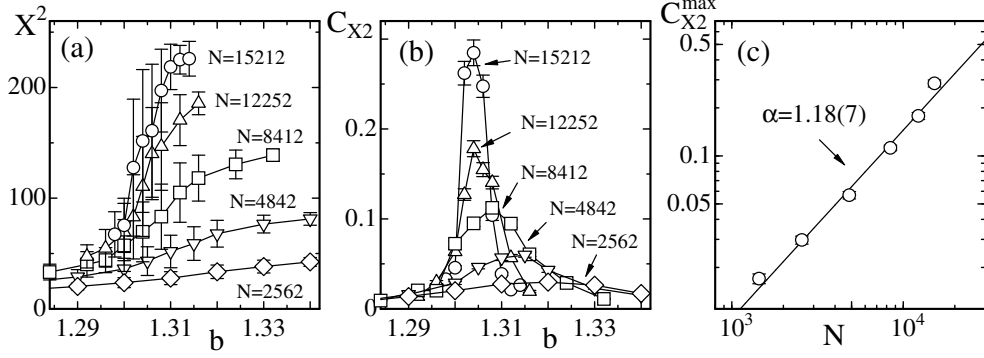


Fig. 5. (a) The mean square size X^2 vs. b , (b) the variance C_{X^2} vs. b , and (c) a log-log plot of the peak $C_{X^2}^{\max}$ vs. N . The solid lines connecting the data in (a),(b) are drawn to guide the eyes. The straight line in (c) is drawn by fitting the data to Eq. (22).

The mean square size X^2 is defined by

$$X^2 = \frac{1}{N} \sum_i (X_i - \bar{X})^2, \quad \bar{X} = \frac{1}{N} \sum_i X_i, \quad (20)$$

where \bar{X} is the center of mass of the surface. The large errors in X^2 reflects a large fluctuation of X^2 as a result of the crumpling transition between the smooth phase and the crumpled phase (Fig. 5(a)). The variance C_{X^2} of X^2 defined by

$$C_{X^2} = \frac{1}{N} \left\langle (X^2 - \langle X^2 \rangle)^2 \right\rangle \quad (21)$$

can reflect the phase transition. The peak at $b \simeq 1.303$ in Fig. 5(b) indicates the existence of the transition. The peak values $C_{X^2}^{\max}$ scales against N ; the straight line in Fig. 5(c) is drawn by fitting the data to

$$C_{X^2}^{\max} \sim N^\alpha, \quad \alpha = 1.18 \pm 0.07. \quad (22)$$

The obtained exponent $\alpha = 1.18(7)$ indicates that the transition is of first-order.

We find from the plot of the series $\{X^2\}$ in Fig. 6(a) that the smooth and crumpled phases are clearly separated. This series is obtained at the transition point $b = 1.304$ on the $N = 15212$ surface. Plots of $\{X^2\}$ similar to the one in Fig. 6(a) are obtained on the $N = 12252$ and $N = 8412$ surfaces, though they are not depicted. In order to have the Hausdorff dimension H defined by $X^2 \sim N^{2/H}$, we calculate the mean values of X^2 in the smooth and crumpled phases independently from the series $\{X^2\}$. On the surfaces $N \geq 8412$, we use a series $\{X^2\}$ at the transition point like the one in Fig. 6(a), while on the surfaces $N \leq 4842$ we use two different $\{X^2\}$ obtained in the smooth and crumpled phases. Figure 6(b) shows the results X^2 vs. N in a log-log scale.

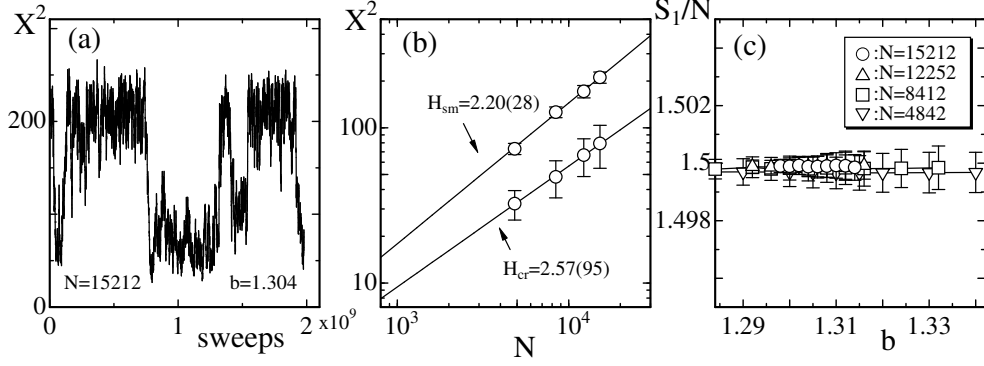


Fig. 6. (a) The variation of X^2 against MCS at the transition on the $N = 15212$ surface, (b) log-log plots of X^2 vs. N in the smooth and crumpled phases at the transition point, (c) S_1/N vs. b .

From the slope of the fitted lines, we have

$$H_{\text{sm}} = 2.20 \pm 0.28 \text{ (smooth)}, \quad H_{\text{cr}} = 2.57 \pm 0.95 \text{ (crumpled)}. \quad (23)$$

These values are comparable to the results $H_{\text{sm}} = 2.02(14)$ and $H_{\text{cr}} = 2.59(57)$ of the conventional model within the errors [28].

We see the expected relation $S_1/N = 1.5$ in Fig. 6(c). This implies that the equilibrium configurations are correctly obtained under the treatment \sum_C in Z .

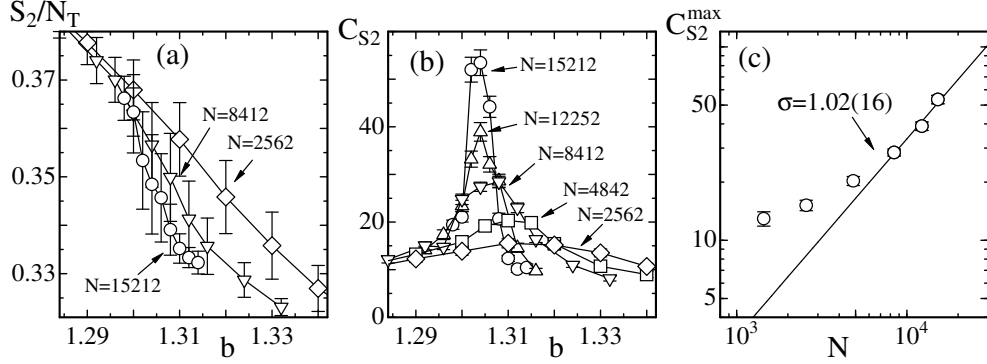


Fig. 7. (a) The bending energy S_2/N_T vs. b , (b) the specific heat C_{S_2} vs. b , and (c) a log-log plot of the peak values $C_{S_2}^{\text{max}}$ vs. N . The fitting is performed by using the largest three data in (c).

The bending energy S_2/N_T , the specific heat

$$C_{S_2} = \frac{b^2}{N} \langle (S_2 - \langle S_2 \rangle)^2 \rangle, \quad (24)$$

and the peak values $C_{S_2}^{\text{max}}$ are plotted in Figs. 7(a)–7(c). By fitting the largest three values of $C_{S_2}^{\text{max}}$, we have

$$C_{S_2}^{\text{max}} \sim N^\sigma, \quad \sigma = 1.02 \pm 0.16. \quad (25)$$

The exponent $\sigma = 1.02(16)$ also confirms that transition is of first-order, and the value is in good agreement with $\sigma = 0.93(13)$ of the conventional model [28].

3.2 A Finsler geometric model

In this subsection, we study a non-trivial model, which is defined by

$$\begin{aligned}
Z(b) &= \int Dg \int \prod_{i=1}^{N_T} d\rho_i \int' \prod_{i=1}^N dX_i \exp[-(S_1 + bS_2 + \lambda_3 S_3 + \lambda_4 S_4)], \\
\int Dg &= \sum_{\mathcal{C}} \int \prod_{i=1}^{N_B} dL_i \exp\left(-\lambda_L \sum_{i=1}^{N_B} L_i^2\right) \int \prod_{i=1}^{N_B} dv_i \exp\left(-\lambda_v \sum_i 1/v_i^2\right), \\
S_1 \text{ and } S_2 &= \text{Eqs. (12), (13), (14),} \\
S_3 &= \sum_{i=1}^{N_T} \rho_i A_i, \quad S_4 = \sum_{ij} |\rho_i - \rho_j|.
\end{aligned} \tag{26}$$

In this model, the variable φ for the deficit angle is suppressed for simplicity, and hence the variable F in Eq. (16) is only given by $F_3 = (L_1^2 + L_2^2 - L_3^2)/2$. In this case the metric g_{ab}^R in Eq.(7) is identical with the conventional Regge metric [21,22,23]

The symbol ρ_i in S_3 is a scalar field on M , which is a conjugate variable to the surface area A_i , and S_4 is the interaction term. \sum_{ij} in S_4 is the sum over all nearest neighbor triangles i and j . The coefficients λ_3 and λ_4 are fixed to $\lambda_3 = \lambda_4 = 1$. The variable ρ_i and the terms S_3 and S_4 are not always necessary but they are introduced to take an in-plane deformation into account. In this model, ρ interacts with the surface through the coupling $\rho_i A_i$. To the contrary, a constant scalar field ρ has no explicit interaction with the surface. If A_i is constant, then the field ρ and hence both S_3 and S_4 are independent of the surface geometry.

The effective Hamiltonian S' including the measure terms is given by $S' = S_1 + bS_2 + \sum_i L_i^2 + \sum_i \tilde{v}_i^2 + S_3 + S_4$, where L_i is the Euclidean bond length. In this expression, we replace $1/v_i$ with the inverse velocity $\tilde{v}_i = 1/v_i$ for numerical simplicity. The variables summed over in the partition function are X , L , \tilde{v} , and \mathcal{C} . One MCS consists of N updates of X , N_B updates of L , N_B updates of \tilde{v}_i , and N_T updates of \mathcal{C} .

The variables L is updated such that $L' = L + \delta L (> 0)$ with random numbers $\delta L \in [-0.5, 0.5]$. In this update, L' is constrained to satisfy the triangle equalities. The inverse velocity $\tilde{v}_i (i = 1, 2)$ is updated such that $\tilde{v}'_i = \tilde{v}_i + \delta \tilde{v}_i (> 0)$

with a random number $\delta\tilde{v}_i \in [-0.5, 0.5]$. None of the variables \tilde{v}_i is updated on the bond 12 of the configuration in Fig. 4(a), one of \tilde{v}_i is updated in Fig. 4(b), and both of the variables are updated in Fig. 4(c). The constraint $\tilde{v}_i < 1$ is imposed. Without this constraint, the acceptance rate for the update of local coordinate \mathcal{C} remains very small (10% \sim 15%), while it remains 40% \sim 50% under the constraint.

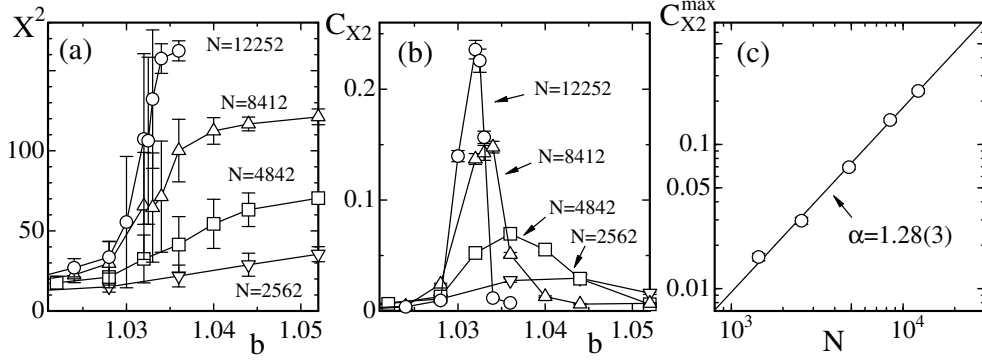


Fig. 8. (a) The mean square size X^2 vs. b , (b) the variance C_{X^2} vs. b , and (c) a log-log plot of the peak values $C_{X^2}^{\max}$ vs. N , where $\lambda_3 = \lambda_4 = 1$.

The mean square size X^2 against b in Fig. 8(a) is almost identical to that of the Euclidean model in the previous subsection. The variance C_{X^2} and the peak value $C_{X^2}^{\max}$ shown in Figs. 8(b) and 8(c) are also almost identical to those of the previous subsection. The straight line in Fig. 8(c) is drawn by fitting the data to Eq. (22), and we have $\alpha = 1.28 \pm 0.03$. This value is identical to the one in Eq. (22) within the error.

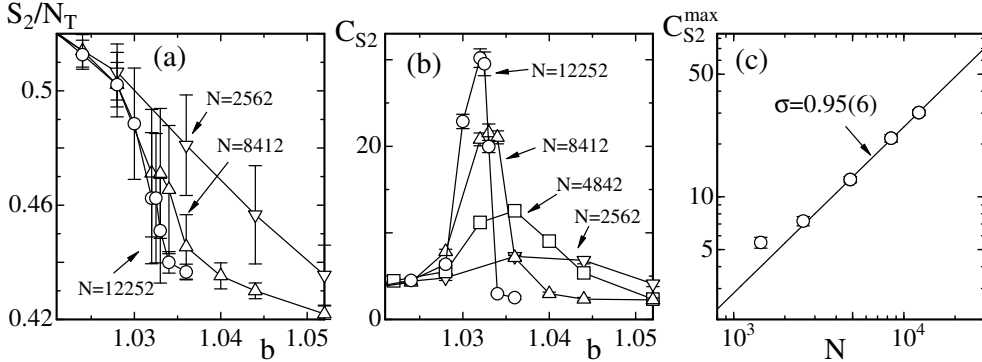


Fig. 9. (a) The bending energy S_2/N_T vs. b , (b) the specific heat C_{S_2} vs. b , and (c) a log-log plot of the peak values $C_{S_2}^{\max}$ vs. N , where $\lambda_3 = \lambda_4 = 1$.

The bending energy S_2/N_B , the specific heat C_{S_2} are almost identical with those of the Euclidean model (Figs. 9(a),(b)). The scaling of $C_{S_2}^{\max}$ predicted in Eq. (25) gives the exponent $\sigma = 0.95(6)$, which is almost comparable to that of the Euclidean model. The Hausdorff dimension H is calculated from the series of $\{X^2\}$ at the transition, and the results are $H_{\text{sm}} = 2.12(20)$ and $H_{\text{cr}} = 3.0(10)$. The result $H_{\text{sm}} = 2.12(20)$ is comparable the one in the previous subsection, while $H_{\text{cr}} = 3.0(10)$ is slightly larger the corresponding result in

the previous subsection. However, we see no difference in the phase structures between the Finsler and conventional models. This implies that the Finsler geometric treatments including \sum_c are well-defined.

We performed the simulations for a model with the variable F , which corresponds to the deficit angle φ of the triangles in M . This model is identical with the one in this subsection except the variable F . The results are consistent with those of the conventional model just like the models shown in this and the preceding subsections.

3.3 Anisotropic surface model

In this subsection, we see that a tubular surface is obtained under a constant vector field on the surface. Let g_{ab}^R in Eq. (7) be $g_{ab}^R = \delta_{ab}$ and $|v_x| = v_{12} = v$, $|v_y| = v_{13} = 1$, where (x, y) is a local coordinate along \mathbf{v} on M , then we have $S_2 = (1/2) \int dx dy [(1/v)(\partial_x n^\mu)^2 + v(\partial_y n^\mu)^2]$. Thus we have an anisotropic bending rigidity such that $b_x = b/v$ and $b_y = bv$. If $v < 1$, then we have $b_x > b_y$, and consequently the surface becomes smooth (wrinkled) in the x direction (y direction) in a certain range of b . In this model, a tubular surface is expected at sufficiently large or small v , although none of the parameters b_x , b_y can be exactly 0.

Thus we have anisotropic bending rigidities b_x and b_y if the vector field \mathbf{v} is constant. Since a vector field \mathbf{v} on M corresponds to the one on the surface $X(M) \subset \mathbf{R}^3$, we assume a constant in-plane tilt order $\vec{\sigma}$ at the center of each triangle. This in-plane variable $\vec{\sigma}$ becomes a vector field on $X(M)$ and corresponds to \mathbf{v} in M .

The variable $\vec{\sigma}$ is of unit length $|\vec{\sigma}| = 1$ and has a value in \mathbf{R}^3 . The direction

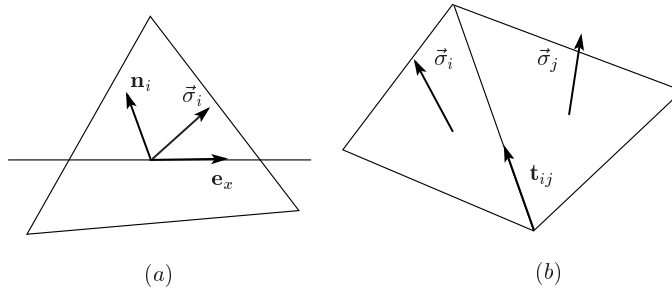


Fig. 10. (a) The x -direction component $\vec{\sigma}_i$ defined by Eq. (27), a unit normal vector \mathbf{n}_i , and the canonical basis vector $\mathbf{e}_x = (1, 0, 0)$, of the triangle i , (b) the variables $\vec{\sigma}_i$ and $\vec{\sigma}_j$ of the triangles i and j , and a unit tangential vector \mathbf{t}_{ij} of the bond ij .

of $\vec{\sigma}_i$ of the triangle i is defined by the projection of $\mathbf{e}_x = (1, 0, 0) \in \mathbf{R}^3$ on the

triangle plane (Fig. 10(a)) such that

$$\vec{\sigma}_i = \frac{\mathbf{e}_x - (\mathbf{e}_x \cdot \mathbf{n}_i)\mathbf{n}_i}{|\mathbf{e}_x - (\mathbf{e}_x \cdot \mathbf{n}_i)\mathbf{n}_i|}, \quad (27)$$

where \mathbf{n}_i is a unit normal vector. As the surface shape varies, not only \mathbf{n}_i but also $\vec{\sigma}_i$ varies. We use the word "constant" in the sense that $\vec{\sigma}_i$ is defined by a constant vector $\mathbf{e}_x = (1, 0, 0)$. This $\vec{\sigma}_i$ represents a constant in-plane tilt order.

The variable $\vec{\sigma}_i$ plays a role of \mathbf{v} on the surface, and therefore the component $\vec{\sigma}_i \cdot \mathbf{t}_{ij}$ is used to define the bending rigidity at the bond ij , where \mathbf{t}_{ij} is a unit tangential vector along the bond ij . The effective bending rigidity b_{ij} is given by $b_{12} = bv_{13}v_{12}^{-1}$ and $b_{13} = bv_{12}v_{13}^{-1}$, where v_{12} and v_{13} are the vectors along the bonds 12 and 13 in Fig. 1(a). However, this b_{ij} becomes singular if $v_{ij} = 0$. For this reason, we simply define v_{ij} by multiplying the integer N_v so that v_{ij} has an integer value in $\{1, 2, \dots, N_v\}$:

$$v_{ij} = 1 + [\sigma_{ij}], \quad \sigma_{ij} = N_v |\vec{\sigma}_i \cdot \mathbf{t}_{ij}|, \quad (\text{case 1}), \quad (28)$$

where $[x]$ represents the integer $\text{Max}\{n \in \mathbf{Z} | n \leq x\}$. Consequently, the minimum (maximum) value of the effective bending rigidity becomes b ($N_v b$).

Another possible discretization of b_{ij} is given by modifying b_{ij} from the naive discretization $b_{12} = bv_{13}v_{12}^{-1}$ and $b_{13} = bv_{12}v_{13}^{-1}$ to $b_{12} = bv_{12}^{-1}$ and $b_{13} = bv_{13}^{-1}$, and by defining v_{ij}^{-1} such that

$$v_{ij}^{-1} = \begin{cases} 1 & (|\vec{\sigma}_i \cdot \mathbf{t}_{ij}| < 0.5) \\ b_0 & (|\vec{\sigma}_i \cdot \mathbf{t}_{ij}| \geq 0.5) \end{cases}, \quad (\text{case 2}), \quad (29)$$

where $b_0 (< 1)$ is a constant to be fixed. It is possible to define v_{ij}^{-1} in Eq.(29) by using $(1/2)(\vec{\sigma}_i + \vec{\sigma}_j) \cdot \mathbf{t}_{ij}$. In this case, v_{ij}^{-1} is uniquely defined on the bond ij ($v_{ij} = v_{ji}$), and hence it is possible to assume the conventional discretization for S_2 , where \sum_C is not included in the partition function Z . However, we use v_{ij}^{-1} in Eq. (29) as a demonstration, where \sum_C is included in Z .

The partition function Z , the Gaussian bond potential S_1 and the bending energy S_2 are given by

$$\begin{aligned}
Z(b) &= \sum_{\mathcal{C}} \int' \prod_{i=1}^N dX_i \exp[-(S_1 + bS_2)], \\
S_1 &= \sum_{\Delta} S_1(\Delta), \quad S_2 = \sum_{\Delta} S_2(\Delta), \\
S_1(\Delta) &= (X_2 - X_1)^2 + (X_3 - X_1)^2, \\
S_2(\Delta) &= \frac{v_{13}}{v_{12}} (1 - \mathbf{n}_0 \cdot \mathbf{n}_1) + \frac{v_{12}}{v_{13}} (1 - \mathbf{n}_0 \cdot \mathbf{n}_2), \quad (\text{case 1}), \\
S_2(\Delta) &= v_{12}^{-1} (1 - \mathbf{n}_0 \cdot \mathbf{n}_1) + v_{13}^{-1} (1 - \mathbf{n}_0 \cdot \mathbf{n}_2), \quad (\text{case 2}),
\end{aligned} \tag{30}$$

where the surface tension coefficients $a_{12} = v_{12}v_{13}^{-1}$ and $a_{13} = v_{13}v_{12}^{-1}$ of $S_1(\Delta)$ are fixed to 1 for simplicity. The unit normal vectors $\mathbf{n}_0, \mathbf{n}_1, \mathbf{n}_2$ in $S_2(\Delta)$ are those shown in Fig. 3(c). Due to the coefficient $b_{ij} (= v_{13}v_{12}^{-1}, \dots, v_{13}^{-1})$ in $S_2(\Delta)$, we have the effective bending rigidity bb_{ij} as mentioned above.

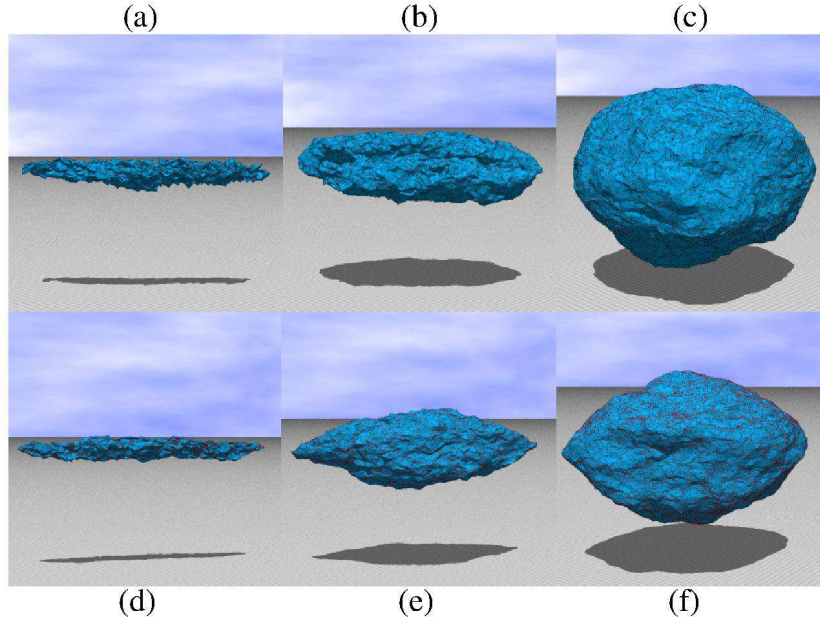


Fig. 11. Snapshot of surfaces of size $N=10242$ of case 1 model obtained at (a) $b=1$, (b) $b=2$, and (c) $b=5$, where $N_v=10$. Snapshots of case 2 model obtained at (d) $(b_0, b) = (0.2, 3.5)$, (e) $(b_0, b) = (0.2, 7.5)$ and (f) $(b_0, b) = (0.2, 15)$.

The integer N_v is fixed to $N_v=10$ in case 1, and the parameter b_0 is fixed to $b_0=0.2$ in case 2, while b is varied in the simulations. Snapshots in Figs.11(a)–(f) show that tubular surfaces are obtained in both case 1 ((a)–(c)) and case 2 ((d)–(f)). Since a vector field on a sphere has singular points, the variable σ_i becomes singular on the surface. Under the condition of Eq. (27), we expect that there appear two singular points. Indeed, these two points can easily be seen at two terminal points of the surface in the snapshots at relatively small b in both case 1 and case 2.

4 Summary and Conclusion

We have numerically studied a Finsler geometric (FG) surface model, which is defined by a mapping X from a two-dimensional Finsler space M to \mathbf{R}^3 . The FG surface model is obtained from the model of Helfrich and Polyakov (HP) for strings and membranes by replacing the Riemannian metric with a Finsler metric $g_{ab}^F(x, y)$. In this sense, this model is an extension of the HP model. By discretizing this continuous FG model, we have a discrete FG model. The discrete Finsler length depends on the direction of local coordinates on the surface, where a new fictitious variable \mathcal{C} is introduced. The variable \mathcal{C} represents a coordinate on the triangles.

To check whether the FG model is well-defined, we firstly study the most simple model without the variable \mathbf{v} , where $g_{ab}^F(x) = \delta_{ab}$. In this model, the crumpling transition between the crumpled and smooth phases is found to be of first-order and is identical to that of the conventional model. It is also found that a FG surface model with random vector field \mathbf{v} has the same phase structure as the conventional model. To demonstrate that a tubular surface appears, we define $g_{ab}^F(x)$ by using a constant vector field \mathbf{v} . The Monte Carlo results show that a tubular surface is obtained in a certain range of the bending rigidity b . Thus, we confirm that an interaction between the surface and an anisotropic vector field is a possible origin of the surface anisotropy.

It is interesting to study an anisotropic surface model with a vector field \mathbf{v} which is not constant or random but dynamically changed. A variable $\vec{\sigma}$ can be defined at the vertices of triangles as a tilt such that its in-plane component plays a role of a vector field on $X(M)$, and interactions between the tilts $\vec{\sigma}$ can also be assumed. The fictitious variable \mathcal{C} is summed over in the partition function of the models in this paper, however, it can be summed over in the discrete Hamiltonians as in the conventional treatment of surface models. Studies on the FG surface model should be performed more extensively.

Acknowledgment

The authors thank Hiroki Mizuno for his support of computer analyses. This work is supported in part by a Promotion of Joint Research of Toyohashi University of Technology.

References

- [1] F. David, in Statistical Mechanics of Membranes and Surfaces, Second Edition, edited by D. Nelson, T. Piran, and S. Weinberg, (World Scientific, 2004) p.149.
- [2] W. Helfrich, Z. Naturforsch **28c** (1973) 693.

- [3] A.M. Polyakov, Nucl. Phys. B **268** (1986) 406.
- [4] L. Radzihovsky, in Statistical Mechanics of Membranes and Surfaces, Second Edition, edited by D. Nelson, T. Piran, and S. Weinberg, (World Scientific, 2004) p.275.
- [5] K.J. Wiese, *Phase Transitions and Critical Phenomena 19*, C. Domb, and J.L. Lebowitz Eds. (Academic Press, 2000) p.253.
- [6] M. Bowick and A. Travesset, Phys. Rep. **344** (2001) 255.
- [7] L. Peliti and S. Leibler, Phys. Rev. Lett. **54** (1985) 1690.
- [8] F. David and E. Guitter, Europhys. Lett. **5** (1988) 709.
- [9] H. Kleinert, Phys. Lett. B **174** (1986) 335.
- [10] Y. Kantor, M. Kardar and D.R. Nelson, Phys. Rev. Lett. **57**, 791 (1986).
- [11] Mehran Kardar and David R. Nelson, Phys. Rev. A **38** (1988) 966.
- [12] L. Radzihovsky and J. Toner, Phys. Rev. Lett **75**, 4752 (1995).
- [13] L. Radzihovsky and J. Toner, Phys. Rev. E **57**, 1832 (1998).
- [14] M. Bowick, M. Falcioni and G. Thorleifsson, Phys. Rev. Lett. **79**, 885 (1997).
- [15] K. Essafi, J.-P. Kownacki, and D. Mouhanna, Phys. Rev. Lett. **106**, 128102 (2011).
- [16] H. Koibuchi, Phys. Rev. E. **77**, 061105(1-5) (2007).
- [17] H.-G. Döbereiner and U. Seifert, Europhys. Lett. **36**, 325 (1996).
- [18] M. Matsumoto, (in Japanese) in Keiryō Bibun Kikagaku, (Shokabou, Japan 1975).
- [19] G.Yu. Bogoslovsky, H.F. Goenner, Phys. Lett. A **244**, 222 (1998).
- [20] T. Ootsuka and E. Tanaka, Phys. Lett. A **374**, 1917 (2010).
- [21] T. Regge, Nuovo Cim. **19** (1961) 45.
- [22] H. W. Hamber, in *Critical Phenomena, Random Systems, Gauge Theories*, Proc. of the Les Houches Summer School 1984, eds. Osterwalder and R. Stora, (North-Holland, 1986).
- [23] F. David, *Simplicial Quantum Gravity and Random Lattices*, Les Houches lecture 1992, arXiv:hep-th/9303127.
- [24] H. Koibuchi, Nucl. Phys. B **836**, 186 (2010).
- [25] J.-P. Kownacki and H. T. Diep, Phys. Rev. E **66** (2002) 066105.
- [26] Y. Nishiyama, Phys. Rev. E **70** (2004) 016101.
- [27] J.-P. Kownacki and D. Mouhanna, Phys. Rev. E **79**, 040101(R) (2009).
- [28] H.Koibuchi and T.Kuwahata, Phys. Rev. E **72**, 026124(1-6) (2005).